IEEE Access
Multidisciplinary | Rapid Review | Open Access Journal

Received 8 February 2025, accepted 9 March 2025, date of publication 17 March 2025, date of current version 1 April 2025.

Digital Object Identifier 10.1109/ACCESS.2025.3552065

RESEARCH ARTICLE

Neural Networks for Phase Shift Optimization of Reconfigurable Intelligent Surfaces Under Imperfect Channel State Information

PABLO FONDO-FERREIRO[1], FIROOZ B. SAGHEZCHI[2], (Senior Member, IEEE), FELIPE GIL-CASTIÑEIRA[1], AND JONATHAN RODRIGUEZ[3], (Senior Member, IEEE)

[1]Information Technologies Group, atlanTTic, Universidade de Vigo, 36310 Vigo, Spain
[2]Chair for Distributed Signal Processing, RWTH Aachen University, 52074 Aachen, Germany
[3]Instituto de Telecomunicações, 3810-193 Aveiro, Portugal

Corresponding author: Pablo Fondo-Ferreiro (pfondo@gti.uvigo.es)

This work was supported in part by Xunta de Galicia, Spain, under Grant ED481B-2022-019 and Grant ED431C 2022/04; in part by the Ministerio de Ciencia, Innovación y Universidades, Spain, under Grant PID2023-148214OB-C22; and in part by the Universidade de Vigo/CISUG for Open Access Charge.

ABSTRACT Reconfigurable intelligent surface (RIS) is a key enabling technology for the sixth generation (6G) of mobile networks. It can focus the signal at an intended location (e.g., a user hotspot) through dynamically adjusting the phase shifts of its passive reflecting elements, thereby enhancing the signal quality and network coverage. However, the optimal configuration of the phase shift profile of RIS is challenging since it requires accurate channel state information (CSI), which is prohibitively expensive to acquire in practice because the number of reflecting elements in RIS is usually large. To address this limitation, in this paper, we train and test a fully-connected neural network (FCN) that estimates the optimal phase shift profile of RIS from noisy CSI measurements. We evaluate the performance of the proposed Machine Learning (ML) model in terms of different key performance indicators (KPIs), including the system bit error rate (BER) and throughput, phase shift estimation mean square error (MSE), and the training time of the neural network itself. Simulation results demonstrate that our proposed technique can significantly improve the performance in RIS-assisted wireless networks, reducing the gap to the optimal network throughput to below 1 %.

INDEX TERMS 6G, reconfigurable intelligent surface (RIS), phase shift optimization, imperfect channel state information (CSI), bit error rate (BER), machine learning, neural network.

I. INTRODUCTION

Reconfigurable intelligent surface (RIS) has gained considerable traction recently, and it is considered as a promising technology for the sixth-generation (6G) of mobile networks. It intelligently manipulates the wireless propagation channel through adjusting the phase shift of its reflecting elements in real-time according to the variations of the channel impulse response [1]. One of the most remarkable use cases of RIS is to increase the network coverage, which is particularly interesting for millimeter wave (mmWave) and terahertz (THz) indoor/outdoor communication systems, which are highly susceptible to radio blockages by moving objects [2].

The phase shift of each RIS element can be independently configured through software so that all reflected signals from these elements arrive at the receiver with the same phase. Therefore, they constructively interfere with each other, thus improving the channel quality between the transmitter (Tx) and the receiver (Rx). However, configuring RIS phase shift profile requires an accurate channel state information (CSI), which is a costly and complex process [3] as we need to estimate the channel for each RIS element, which involves a tremendous number of pilot signals and sophisticated algorithms for channel estimation. Therefore, practical RIS

The associate editor coordinating the review of this manuscript and approving it for publication was Yeon-Ho Chung.

channel estimation techniques naturally have to deal with inherent errors derived from either a reduced number of pilots per RIS element, a less frequent CSI estimation, or a quantized CSI feedback. However, the use of this inaccurate CSI for RIS phase shift configuration can considerably degrade the system performance [4].

To address this problem, in this paper, we propose a novel two-stage approach for RIS phase shift optimization. In the first stage, the RIS channel is roughly estimated using an affordable technique, e.g., a reduced number of pilot signals, accurate but less frequent (outdated) CSI measurements, or naive channel estimation algorithms (e.g., Least Squares technique). Then, in the second stage, these inaccurate CSI measurements are fed into a fully-connected feed-forward neural network (FCN) to learn from the channel regularities (i.e., temporal and spatial correlations in the channel impulse response) to estimate the amount of phase shift for each RIS element. It is worth noting that our proposed approach does not require to estimate the full channel response of the RIS (i.e., both amplitude and phase response across all subcarriers). Instead, it estimates only a single phase shift value per RIS element. This significantly reduces the complexity of the employed FCN model while still considerably improving the system performance.

In detail, our main contributions can be summarized as follows:

- We develop an FCN-based technique for predicting optimal RIS phase shift configurations from imperfect CSI. Note that we are not introducing a novel technique for RIS channel estimation, rather our approach optimizes the RIS phase shift profile leveraging rough CSI measurements, acquired by less expensive channel estimation procedures.
- We provide extensive simulation results to evaluate the system performance of our proposed RIS phase shift optimization technique in terms of bit error rate (BER), throughput, channel estimation mean square error (MSE), and the training time of the neural network.
- We compare the results against three different benchmarks: 1) using a random phase shift configuration; 2) directly using the imperfect CSI without any denoising; and 3) using perfect CSI as an optimum bound. The results show the strong potential of our proposed approach.

After this introduction, the paper is structured as follows. Section II summarizes the related work. Section III defines our system model. Section IV introduces our proposed solution, and Section V presents the simulation results. Finally, Section VI concludes this paper.

II. RELATED WORK

In this work, we address RIS phase shift optimization from imperfect CSI estimations using a neural network. Since our proposed solution requires the use of existing CSI estimation procedures for obtaining the imperfect CSI measurements, in this section we first review the main approaches in the literature for RIS channel estimation. Then, we review the state of the art techniques for RIS phase shift optimization.

A. CHANNEL ESTIMATION FOR RIS

In order to properly configure RIS phase shift profile, it is important to have an accurate estimation of the cascaded channel (i.e., transmitter-RIS-receiver). Two main categories of techniques exist for RIS CSI acquisition [2]: 1) equipping RIS with active radio frequency (RF) chains to enable pilot transmission or processing capabilities at the RIS; and 2) estimating the cascaded channel at the receiver by configuring the RIS to given reflection patterns (e.g., enabling or disabling some RIS elements), transmitting pilot signals from the transmitter, and estimating the cascaded channel at the receiver.

The first category of works involves active RF chains in the RIS, which is costly and unsustainable in terms of hardware development and energy consumption. Regarding the second category, early works, e.g., [5], [6], focused on simply turning on and off the individual RIS elements. However, this approach is time-consuming and require a tremendous number of pilot signals since the channel estimation procedure has to be repeated for every RIS element one by one. To overcome this limitation, the authors of [7] propose a protocol to jointly execute channel estimation and phase shift optimization in passive RIS. The cascaded channel is estimated at the receiver based on the pilot signals sent by the transmitter. The optimization is based on aligning the RIS phase shifts to the tap index with the strongest channel impulse response (CIR).

Other approaches in this second category involve the use of a deep learning (DL) framework for RIS channel estimation. In [8], the authors designed a twin convolutional neural network (CNN) architecture, using as input the received pilot signals to estimate the direct and the cascaded channel. Each user provides its received pilot signals to the deep learning network, to estimate its own channel. The proposed model introduces a new DL architecture for channel estimation by combining both convolutional and fully connected layers together. In contrast, conventional DL models for channel estimation in massive MIMO systems have typically relied on either an FCN [9] or a CNN [10], but not a combination of both.

Last but not least, unlike the aforementioned RIS channel estimation techniques, which estimate only the cascaded channel, the authors in [11] proposed a pilot-assisted technique to estimate not only the cascaded channel, but also each of its individual components (i.e., Tx-RIS and RIS-Rx channels). They formulate the problem as a combined sparse matrix factorization and matrix completion problem. It is a two-stage algorithm which includes the bilinear generalized approximate message passing (BiG-AMP) [12] for sparse

matrix factorization and the Riemannian manifold gradient-based algorithm for matrix completion [13].

B. RIS OPTIMIZATION

The optimization of RIS phase shift profile has been approached in the literature in three different ways: physics-based models, heuristic algorithms and machine learning (ML) techniques [14]. The addressed problem relates to controlling the phase shift of each RIS element in order to optimize the system performance in terms of a given KPI, e.g., network sum-rate [15], power consumption [16], or energy consumption [17]. Physics-based solutions rely on exact mathematical models governing the radio signal propagation (e.g., using ray tracing method) [18]. On the other hand, heuristic approaches aim for fast but approximate algorithms that can strike a balance between the algorithmic complexity and the system performance, using e.g., alternating optimization [19] or greedy algorithms [20]. However, most of these works focus on deriving a theoretical limit for the maximum performance and cannot be applied directly in practical systems (e.g., they assume perfect CSI). On the other hand, ML-based phase shift optimization algorithms can operate without the need for an exact mathematical model of the system or accurate CSI measurements as they can learn patterns from labeled channel data or from interactions with the wireless communication environment [21].

ML algorithms have been employed for RIS phase shift control, including supervised learning [22], unsupervised learning [23] and reinforcement learning (RL) [24]. The main challenge of RL approaches is the need for a large number of training epochs for convergence [14]. Unsupervised approaches seem to be more practical for real-world applications since they do not require labeled data to operate, although they still need labeled data for cross-validation and testing. If we just focus on supervised learning approaches for sum rate maximization, which is the basis of our proposal, some solutions leverage user positions as input data [22], [25], exploit temporal channel correlations [26] or quantization of the phase shifts to discrete levels (for finite precision) [27] to reduce the dimension of the ML model. For example, the authors in [22] rely on accurate positioning information for mobile terminals as input for their neural network (NN) model. They also assume that the optimum phase shifts are available during the training phase (as the training data).

Overall, all of the aforementioned works exhibit limitations for their application in practical scenarios (e.g., they require perfect CSI or accurate user location information, or they reveal high computational complexity). In contrast, our approach has none of these limitations and can be adopted in practical systems. In particular, we follow a similar approach as in [22], but we replace the users' accurate positioning information with their inaccurate CSI measurements (which can be obtained from a lower number of pilot signals or from less frequent CSI estimations), which is more practical in real-world mobile systems.

III. SYSTEM MODEL

We consider an indoor scenario for data communication between two single-antenna devices, namely, a transmitter device which sends data to a receiver device (see Fig. 1). We consider a mmWave or THz channel in which the direct channel between the transmitter and the receiver suffers from blockage due to a high attenuation loss (e.g., caused by an obstacle). A square-shaped N-element RIS is employed to enhance the channel between the Tx and Rx. The phase shift of each reflecting element of the RIS can be individually configured with infinite resolution in the range $[0, 2\pi)$. The Tx and RIS are statically placed in the scenario, while the Rx moves through the environment following a random waypoint mobility model [28], starting at a random position of the environment. Notice that this scenario can reflect the situation in which the Tx represents a base station while the RX resembles a UE.

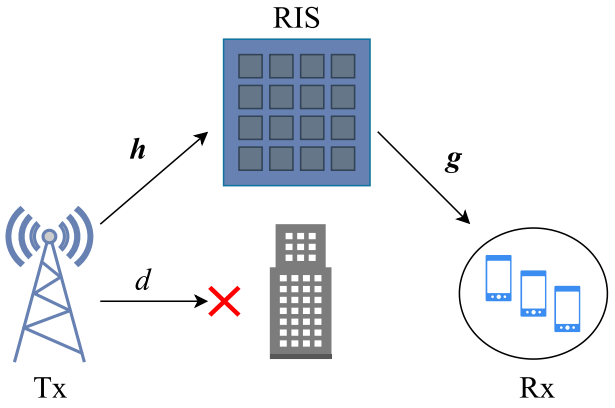

FIGURE 1. System model of our considered scenario.

We use the same cascaded RIS channel model proposed in [29]. Let $\mathbf{h}^\intercal = \{h_1, \ldots, h_N\}$ be the N-element vector with the Tx-RIS channel coefficients, $\mathbf{g} = \{g_1, \ldots, g_N\}$ the N-element vector with the RIS-Rx channel coefficients and d the Tx-Rx direct channel gains. Since we assume that a blockage occurs in the direct channel, we consider $d = 0$. Hence, the received signal y at the receiver is given by

$$y = (\mathbf{g}^\intercal \Phi \mathbf{h} + d)x = (\mathbf{g}^\intercal \Phi \mathbf{h})x, \tag{1}$$

where x is the transmitted signal and Φ is the $N \times N$ diagonal matrix containing the RIS elements' responses, given by

$$\Phi = \begin{bmatrix} \mu_1 e^{j\phi_1} & & & \\ & \mu_2 e^{j\phi_2} & & \\ & & \ddots & \\ & & & \mu_N e^{j\phi_N} \end{bmatrix}. \tag{2}$$

We consider a passive and lossless RIS, i.e., $\mu_i = 1, \ \forall i \in \{1, \ldots, N\}$. Therefore, our decision variables are the phase shifts of the RIS elements ($\phi_i \in [0, 2\pi), \ \forall i \in \{1, \ldots, N\}$).

If the exact CSI values of both Tx-RIS and RIS-Rx channels were known for all reflecting elements, the optimum phase shift configuration of the RIS would be trivial and given by (3), which ensures that the reflected signals from all elements are received at the Rx with perfect phase alignment, so that they constructively interfere with each other.

$$\phi_i = 2\pi - \angle g_i - \angle h_i \; \forall \; i. \tag{3}$$

However, this perfect CSI for the $\mathbf{h}$ and $\mathbf{g}$ channels cannot be obtained in practice because, among other factors, the channel noise variance dictates the Cramer-Rao lower bound for the estimation error, putting aside the pilot overhead needed for the channel estimation for every RIS element during every channel coherence time.

We assume that a lightweight channel estimation procedure (e.g., using a low density of pilot signals) is employed to achieve a rough CSI information. Consequently, the obtained CSI has a certain amount of channel estimation error (CEE). We denote this imperfect CSI values for each element of the Tx-RIS and RIS-Rx channel vectors by $\hat{h}_i = h_i + e$ and $\hat{g}_i = g_i + e$, $\forall i \in \{1, \ldots, N\}$, respectively, where $e \sim \mathcal{CN}(0, \sigma^2)$ is a zero-mean complex Gaussian random variable with variance σ^2, representing the CEE. This imperfect CSI (i.e., $\hat{h}_i$, $\hat{g}_i$, $\forall i \in \{1, \ldots, N\}$) will constitute the input of the neural network that we design in this paper for RIS phase shift optimization.

Our objective is to maximize the system performance by configuring the phase shift of the RIS elements from imperfect CSI estimations. In detail, we aim at maximizing the system throughput (data rate) and BER for the transmissions between the Tx and Rx. The data rate is given by (4):

$$R = B \log_2 (1 + \gamma), \tag{4}$$

where B is the system bandwidth and γ is the signal-to-noise (SNR) ratio given by (5):

$$\gamma = \frac{P\,|(\mathbf{g}^\intercal \Phi \mathbf{h})|^2}{\eta^2}, \tag{5}$$

where P represents the transmit power of the Tx and $w \sim \mathcal{CN}(0,\ \eta^2)$ is a zero-mean complex Gaussian random variable with variance η^2, which models the additive thermal noise power at the receiver.

We consider that the system is using a Quadrature Phase Shift Keying (QPSK) modulation. Hence, the BER is given by

$$\text{BER} = Q\left(\sqrt{2\gamma}\right), \tag{6}$$

where $Q(x)$ is the standard Q-function defined as:

$$Q(x) = \frac{1}{\sqrt{2\pi}} \int_x^\infty \exp\left(-\frac{u^2}{2}\right) du. \tag{7}$$

Table 1 summarizes our assumed CSI in the system.

TABLE 1. Our assumed CSI in the system.

N	Number of RIS elements
σ^2	Variance of the CEE
$\hat{\mathbf{h}} = \{\hat{h_1}, \ldots, \hat{h_N}\}$	Tx-RIS channel estimation with imperfect CSI
$\hat{\mathbf{g}} = \{\hat{g_1}, \ldots, \hat{g_N}\}$	RIS-Rx channel estimation with imperfect CSI

IV. PROPOSED SOLUTION

We propose a novel solution to address RIS phase shift optimization in two stages. In the first one, we use a lightweight technique (e.g., less pilot signals, less frequent CSI measurements or simpler channel estimation algorithms) for obtaining a rough CSI. In the second stage, these inaccurate CSI measurements are fed into our proposed FCN to estimate the optimum phase shift for each RIS element.

For the second stage, we consider a data-driven approach, where we can capture data during an offline training phase. We train a FCN model [30] to predict the optimum phase shift profile and then we use the trained model to make predictions during the online inference phase. As previously stated in Section III, the input data corresponds to the estimated channel vectors for the Tx-RIS ($\hat{\mathbf{h}}$) and RIS-Rx ($\hat{\mathbf{g}}$) channels obtained through lightweight but error-prone channel estimation processes. Since the passive RIS does not alter the amplitude of the signal, we are only interested in the angle of the matrices, thus we use the values of $\angle\hat{h}_i$ and $\angle\hat{g}_i$ rather than $\hat{h}_i$ and $\hat{g}_i$, respectively. The output label of each training example is the optimal phase shift configuration for that scenario, denoted by ϕ^*. In order to properly use this angular data in the neural network, we encode them by calculating the sine and cosine to each angular value, to avoid the issues caused by the circular symmetry of the angles (i.e., they have a periodicity of 2π). In detail, for each individual input and output angular value (θ), we use the following encoding function.

$$\theta \rightarrow (\sin(\theta), \cos(\theta)) \tag{8}$$

Correspondingly, the decoding function to recover the angular value from a pair of encoded values is given by:

$$(y_1, y_2) \rightarrow \arctan\left(\frac{y_1}{y_2}\right). \tag{9}$$

Consequently, the input and output variables of the FCN are shown in Table 2 and Table 3, respectively.

During the offline training phase, we collect samples by placing the receiver at different positions throughout the room. The samples contain channel estimations for the Tx-RIS and RIS-Rx channels, which will be later used as training examples in the dataset. In a practical scenario, to generate the output label for each sample, it is not feasible to obtain the perfect CSI information for each cascaded channel [3]. However, we may obtain the optimum phase

TABLE 2. Input variables of our proposed FCN.

$\{\sin(\hat{h}_1), \ldots, \sin(\hat{h}_N)\}$	Sine of the encoded angles of the Tx-RIS channel estimation with imperfect CSI
$\{\cos(\hat{h}_1), \ldots, \cos(\hat{h}_N)\}$	Cosine of the encoded angles of the Tx-RIS channel estimation with imperfect CSI
$\{\sin(\hat{g}_1), \ldots, \sin(\hat{g}_N)\}$	Sine of the encoded angles of the RIS-Rx channel estimation with imperfect CSI
$\{\cos(\hat{g}_1), \ldots, \cos(\hat{g}_N)\}$	Cosine of the encoded angles of the RIS-Rx channel estimation with imperfect CSI

TABLE 3. Output variables of our proposed FCN.

$\{\sin(\phi_i^*), \ldots, \sin(\phi_N^*)\}$	Sine of the encoded angles of the optimal RIS phase shift configuration
$\{\cos(\phi_i^*), \ldots, \cos(\phi_N^*)\}$	Cosine of the encoded angles of the optimal RIS phase shift configuration

shift configuration for the RIS for that receiver location through an exhaustive search or advanced techniques (e.g., alternating optimization [19]). Note that this latter process is very time-consuming, so it can only be used during the offline training phase, but not for real-time operation. In the real-time online inference phase, after the neural network is trained, we assume that only a lightweight channel estimation process is triggered for every channel coherence time, and the trained FCN is used to predict the optimal phase shift profile of the RIS.

V. RESULTS

A. SCENARIO

For performance evaluation, we consider a scenario with one base station and one mobile user equipment operating in downlink in 73 GHz mmWave frequency band. We used the open source link-level TU Vienna 5G simulator [31] both for generating a dataset and also for evaluating the performance of our proposed FCN for RIS phase shift estimation. We have considered different RIS sizes N (i.e., the number of RIS reflecting elements) and introduced an additional path loss in the transmitter-receiver direct channel to simulate a link blockage (e.g., caused by an obstacle). Hence, the communication between the BS and the UE is possible only through the RIS, as depicted in Fig. 1.

B. DATASET GENERATION

For the sake of reproducibility of our results, we generated different datasets using the link-level TU Vienna 5G simulator. We generated a different dataset for each RIS size considered in our experiments. Then, we split each dataset into training, validation and test sets.

For the dataset generation, in each time slot of the simulation, the TU Vienna 5G simulator generates i.i.d. channel matrices for the Tx-RIS and RIS-Rx channels. The phase shifts of these elements have uniform distribution between $-\pi$ and π (thus they have zero mean and variance 3.289). For each time slot, we calculate the exact phase shift of the RIS elements given by (3), which constitute the output labels in our datasets. Thus, in a real-world setup the output label represents the optimum phase shift configuration for a given user location. We denote the total number of time slots in our simulations (equivalently, the number of distinguished labels in our datasets) as L. These L time slots constitute one channel block. Then, to create our datasets, as depicted in Fig. 2, we sequentially sample each channel block S times, simulating the lightweight channel estimation process. In the process, CEE is added to the actual Tx-RIS and RIS-Rx channel matrices. This CEE has normal distribution with zero mean and variance σ^2. The outcome noisy channel matrices are then fed, as input data, to our proposed FCN model. The variance of the CEE represents the different factors affecting the quality of the lightweight estimation process in a real-world scenario (e.g., noise, fading, multipath).

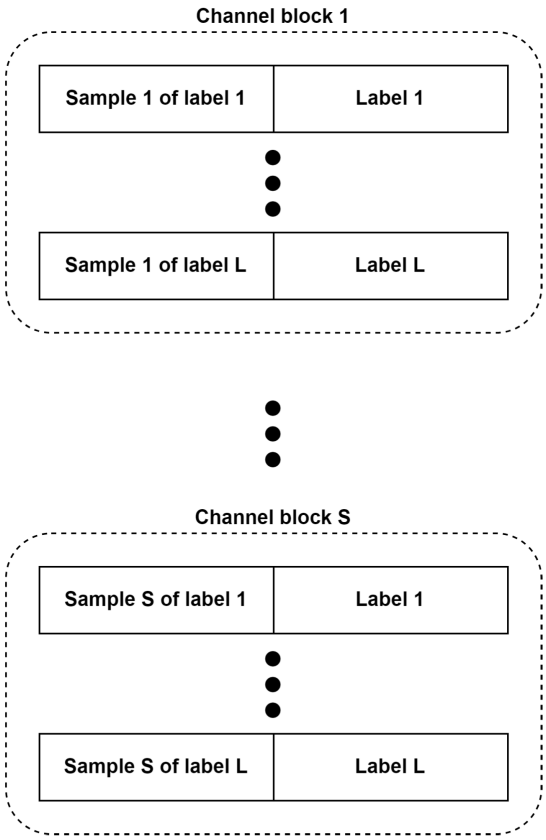

FIGURE 2. Dataset generation process.

The dataset is then split in $70-10-20$ percent ratios for training, validation and testing. Inside each set, the samples are randomly shuffled.

C. BENCHMARKS

We compare the performance of our proposed FCN-based RIS phase shift estimation technique (described in Sec. IV) against the following three benchmark algorithms:

- Random phase shift configuration
- Direct usage of imperfect CSI
- Exact phase shift configuration (assuming perfect CSI)

The random phase shifts considers the random configuration of each phase shift regardless of the CSI. This is the most basic baseline approach for RIS phase shift optimization, which is widely used in the related works, e.g., [32], as a benchmark.

The direct usage of imperfect CSI implies configuring the phase shifts of the RIS elements directly using the measured $\hat{\mathbf{g}}$ and $\hat{\mathbf{h}}$ matrices contaminated with CEE (i.e., raw CSI measurements without any denoising). In detail, the phase shift of each element is given by (10).

$$\hat{\phi}_i = 2\pi - \angle \hat{g}_i - \angle \hat{h}_i \; \forall \, i. \tag{10}$$

The exact phase shifts are used to analyze the gap from other solutions to an idealistic phase shift configuration, assuming perfect CSI is available.

D. PERFORMANCE EVALUATION METRICS

We use the following metrics for performance evaluation:

- Training time: Measures the amount of time required for the training of the FCN.
- Number of epochs used for the training of the FCN.
- Phase shift estimation MSE using the FCN approach: Measures the average of the squares of the prediction errors. The error is defined as the difference between the predicted value and the actual one. If we let $\hat{\phi}$ be the values predicted by the FCN and ϕ^* the true values, we calculate the MSE as follows:

$$\begin{aligned} \text{MSE} = &\frac{1}{N}\sum_{i=1}^{N}(\cos(\hat{\phi}_i) - \cos(\phi_i^*))^2 \\ &+ \frac{1}{N}\sum_{i=1}^{N}(\sin(\hat{\phi}_i) - \sin(\phi_i^*))^2. \end{aligned} \tag{11}$$

- BER of the communication system using the data from the test set, measured using the link-level TU Vienna 5G simulator.
- Throughput of the communication system using the data from the test set, measured using the simulator.

Note that the last two metrics (BER and throughput) measure the RIS-enabled end-to-end communication system performance. Thus, we will use them for assessing the overall system performance of our proposed solution and comparing it with benchmark approaches. In contrast, the first three metrics above are used to assess the performance of the FCN model. Therefore, we will use them for tuning the hyperparameters of our proposed FCN.

E. FCN TRAINING AND HYPERPARAMETER TUNING

For simulations, we used MATLAB on an AMD Ryzen 7 5800H @ 3.20GHz laptop, to process the dataset, train the FCN and provide the prediction results as output. We made publicly available the source code for this processing in [33].

The simulation parameters used for the experiments are detailed in Table 4. We configured the TU Vienna 5G simulator to use the Two-Wave with Diffuse Power (TWDP) channel model [34], which generalizes the Rayleigh and Rician fading models. We set the parameters of the TWDP model as follows: $K = 100$ and $\Delta = 0$.

TABLE 4. Simulation parameters used for the experiments.

Number of RIS elements (N)	$\{4, 16, 64\}$
Variance of the CEE (σ^2)	$\{0.1, 0.2, \ldots, 0.9, 1.0\}$
Number of labels (L)	$\{10, 100\}$
Carrier frequency	73 GHz
Bandwidth (B)	1.08 MHz
Transmitter power (P)	30 dBm
Channel model for $\mathbf{h}$ and $\mathbf{g}$	TWDP ($K = 100$, $\Delta = 0$)

To analyze the best hyperparameters for our proposed FCN approach, we studied the performance of the algorithms for different sets of hyperparameters as presented in Table 5.

Given the complexity of examining every possible combination of parameters, we independently studied the impact on validation performance of each parameter for fixed values of the others, considering different RIS sizes (i.e., 4, 16, and 64 elements).

TABLE 5. Value sweep for neural network hyperparameters.

Training algorithm	SCG, GDM
Number of hidden layers	$\{1, 2, 3, 4, 5\}$
Number of neurons in each hidden layer	$10, \ldots, 500$
Number of samples per label (S)	$\{100, 200, \ldots, 1000\}$
Transfer function for the hidden layer	Hyperbolic tangent sigmoid
Maximum number of training epochs	10000
Maximum number of validation checks[1]	10
Loss function	MSE

We first selected the training algorithm, comparing the performance (measured in terms of phase shift estimation MSE) and training time provided by the Scaled conjugate gradient (SCG) [35] and Gradient descent with momentum (GDM) algorithms, for a RIS size of 4 elements, $L = 100$, $S = 100$, $\sigma^2 = 0.5$, 1 hidden layer with 100 neurons and explored a higher maximum number of epochs of 100000 (it is only relevant for the GDM algorithm, because the SCG converged in less than 1000 epochs). The results, shown in Table 6, reveal that the SCG algorithm achieves almost the

same phase shift estimation MSE as the GDM algorithm, but with two orders of magnitude less training time. This confirms the results reported in previous studies (e.g., [36]) indicating that the SCG algorithm outperforms GDM. Note that we did not explore other training algorithms, since the SCG is one of the fastest. For the rest of this paper, we only use the SCG training algorithm.

TABLE 6. Comparison of the training algorithms.

Algorithm	Learning rate	Training time (s)	Phase shift estimation MSE (rad^2)
SCG	N/A	2.66	0.975
GDM	0.0001	747.26	2.860
GDM	0.001	737.16	1.493
GDM	0.01	715.35	1.001
GDM	0.1	733.23	0.924

Then, we swept the number of hidden layers of the FCN to explore the training time and the phase shift estimation error. We compared the performance in terms of MSE with the direct usage of imperfect CSI for phase shift configuration as a baseline. We executed the experiment for $L = 100$ labels, $S = 1000$ samples per label, and CEE variance of $\sigma^2 = 0.5$. The number of hidden layers varied from 1 and 5, while the number of neurons in each hidden layer varied from 10 to 90 in steps of 20. Fig. 3 shows the phase shift estimation MSE using the FCN and direct approaches. Fig. 4 shows the training time for the FCN approach. The results in the figures show the average of ten independent executions along with 95 % confidence intervals. We only depict the results for a size of $N = 16$ for the sake of brevity, but the results are analogous for the other RIS sizes analyzed (i.e., 4 and 16).

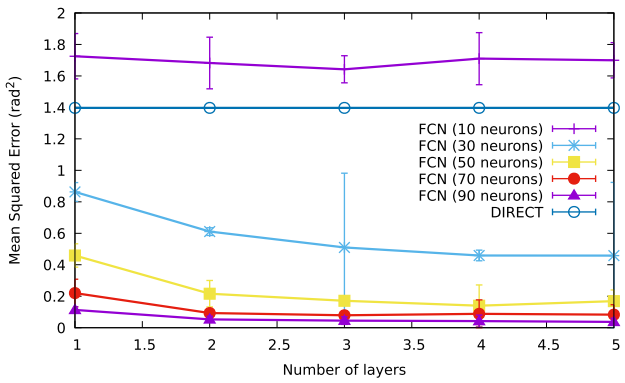

FIGURE 3. Phase shift estimation MSE of the FCN and direct approach for different number of hidden layers and neurons per hidden layer, for a RIS size of $N = 16$.

As expected, increasing the number of hidden layers and the number of neurons per hidden layer reduces the MSE, but conversely results in a longer training time. For any number of hidden layers (between 1 and 5), having only 10 neurons in each hidden layer performs worse than the direct approach. However, any other configuration outperforms that baseline, even for a single hidden layer. The high variability in the training time comes from the early stopping criterion

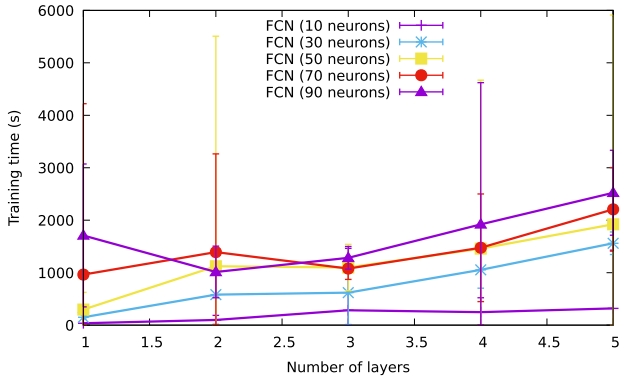

FIGURE 4. Training time of the FCN for different number of hidden layers and neurons per hidden layer, for a RIS size of $N = 16$.

of 10 iterations with increasing validation error (to avoid overfitting). Based on these results, we can observe that the impact of the number of hidden layers on the estimation performance is less than the impact of the number of neurons per hidden layer (e.g., a single layer with 30 neurons outperforms 3 hidden layers with 10 neurons). Moreover, the training time is mostly dependent on the total number of neurons in the FCN. Thus, for the rest of this work, we opt for the simplest model of using just a single hidden layer.

In the next experiment, we explored the impact of the number of neurons in the single hidden layer model. We measured the phase shift estimation MSE and the training time of our proposed FCN. We compared these metrics with the direct approach for different number of neurons, varying from 100 to 500 in steps of 100. The rest of the parameters have been set as follows: $L = 100$, $S = 1000$, $\sigma^2 = 0.5$. The results for the phase shift estimation MSE and training time are shown in Fig. 5 and Fig. 6, respectively.

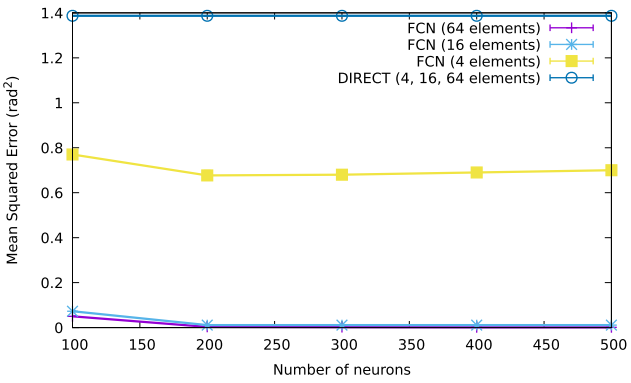

FIGURE 5. Phase shift estimation MSE for the FCN and direct approach for different number of neurons per hidden layer, for three different RIS sizes ($N = 4, 16, 64$).

The phase shift estimation MSE using the FCN-based approach outperforms the direct approach for every number of neurons above 100. Above 200 neurons, it seems that the MSE does not improve, while the training time keeps increasing with the number of neurons. Thus, we can choose

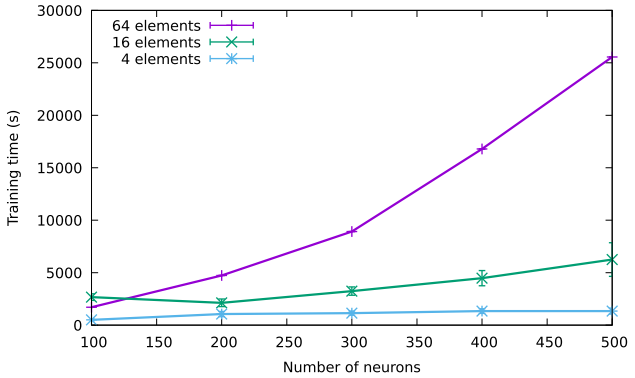

FIGURE 6. Training time of the FCN for different number of neurons in the hidden layer, for three different RIS sizes ($N = 4, 16, 64$).

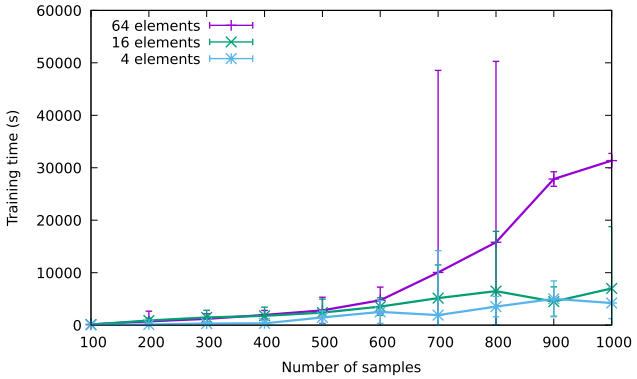

FIGURE 8. Training time of the FCN for different number of CSI samples per data label, for three different RIS sizes ($N = 4, 16, 64$).

200 neurons for the hidden layer as a good trade-off between performance and model complexity.

Finally, we explored the impact of the number of samples for each label (i.e., the number of noisy channel acquisitions for each label) in the prediction quality and training time. We varied the number of samples (S) from 100 to 1000 in steps of 100, while setting the rest of the parameters as follows: $L = 100$ and $\sigma^2 = 0.5$. The results for the MSE and training time are shown in Fig. 7 and Fig. 8, respectively.

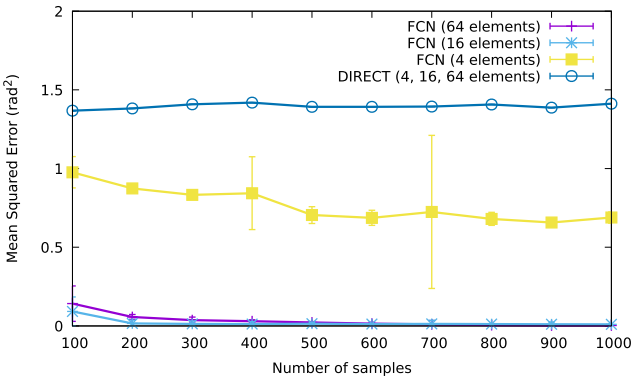

FIGURE 7. Phase shift estimation MSE for the FCN and direct approach for different number of CSI samples per data label, for three different RIS sizes ($N = 4, 16, 64$).

As expected, increasing the number of CSI samples results in a lower MSE but also an increased training time, since the size of the dataset increases proportionally. For values of S below 500 samples, we can observe improvements in terms of MSE, while above that value, the improvements are negligible. We conclude that a value of 500 CSI samples per data label is necessary to get an acceptable level of performance. Therefore, the proposed FCN-based channel denoising is practical in static or quasi-static wireless conditions.

To sum up, after this training process, the final hyperparameters chosen for a good performance of the proposed FCN approach are: SGD training algorithm, a single hidden layer with 200 neurons and $S = 500$ CSI samples per label. These parameters are chosen for the end-to-end system performance evaluation described in the following subsection.

F. END-TO-END SYSTEM PERFORMANCE

After configuring the hyperparameters of the FCN, we performed further experiments to analyze the end-to-end performance of the communication system, evaluating the throughput and BER over the test set.

In the first experiment, we evaluated the throughput and BER of the proposed FCN approach and the benchmark approaches for different values of the CEE variance (σ^2). Fig. 9 and Fig. 10 depict the throughput and BER, respectively, when the number of data labels are fixed at $L = 100$ and σ^2 is varied between 0 and 1.

As expected, the maximum throughput is achieved by the optimum approach (i.e., assuming perfect CSI information is available), while the random phase shift configuration attains the lowest BER. Our FCN-based proposal attains the second best results, outperforming the direct approach for every value of the RIS size evaluated. Obviously, the performance of the optimum and random remain constant regardless of the variance of the CEE since none of them are affected by the channel estimation process. Our proposal outperforms the direct approach in terms of throughput for every value of σ. Interestingly, the performance of our proposed FCN approach increases with the RIS size. For example, in the case of the largest RIS size analyzed (i.e., $N = 64$), our proposal achieves an optimum throughput even for large σ^2 values, in which the communication becomes unfeasible with both the direct and random approaches.

In terms of BER, we can observe a similar behavior, in which the optimum approach obtains the lowest BER, while the random attains the highest BER, as expected. In both FCN-based and direct approaches, the BER grows with σ^2. The FCN-based approach outperforms the direct usage of imperfect CSI for every configuration, with the most notable differences observed for larger RIS sizes (e.g., $N = 64$), in which the BER values obtained by the FCN

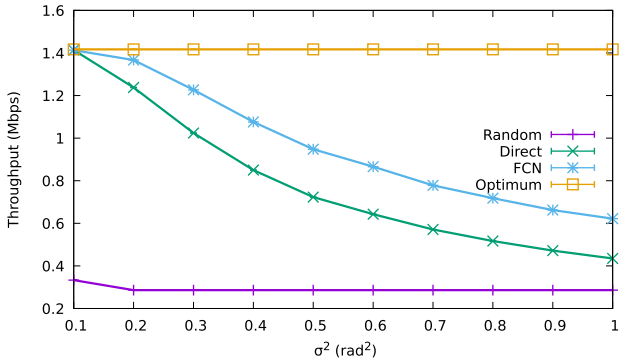

(a) $N = 4$

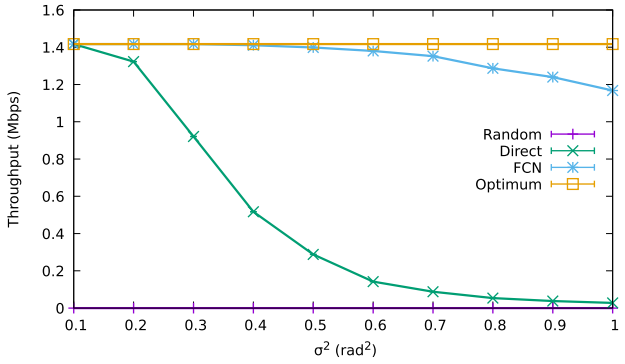

(b) $N = 16$

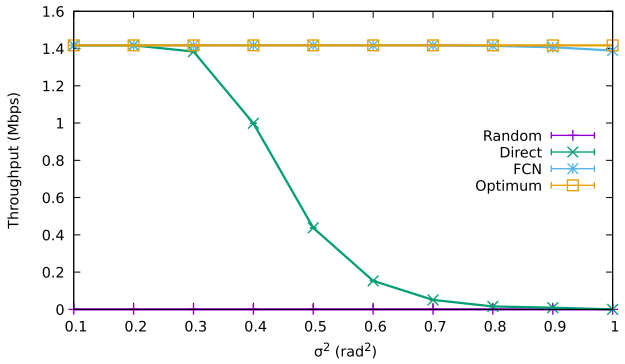

(c) $N = 64$

FIGURE 9. Throughput of the FCN, random, direct and optimum approaches when the CEE variance varies between 0 and 1, for three different RIS sizes ($N = 4, 16, 64$).

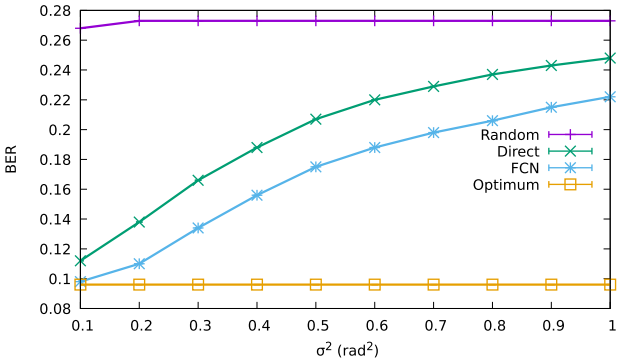

(a) $N = 4$

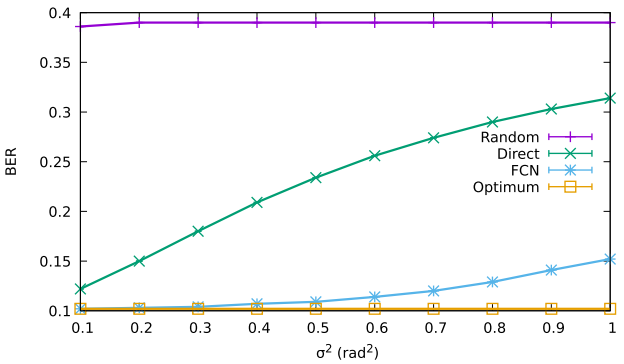

(b) $N = 16$

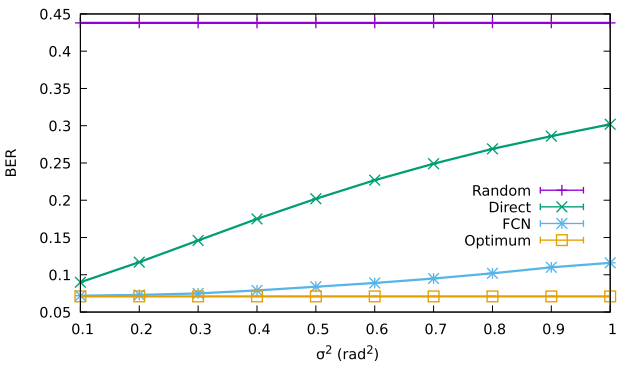

(c) $N = 64$

FIGURE 10. BER of the FCN, random, direct and optimum approaches when the CEE variance varies between 0 and 1, for three different RIS sizes ($N = 4, 16, 64$).

are very close to the optimum, while the direct one quickly diverges.

Finally, we evaluated the throughput and BER values obtained for different approaches while varying the number of labels (L). Fig. 11 and Fig. 12 depict the throughput and BER, respectively, for different values of L with a fixed value of $\sigma^2 = 0.5$.

The results depict a similar trend, in which our proposal behaves very close to the optimum, strongly outperforming the direct and random approaches. For low RIS sizes (e.g., $N = 4$) the performance of our proposal deteriorates (throughput decreases and BER increases) as the number of data labels (L) increases. This result is expected since increasing the number of labels complicates the prediction process of the FCN (it is more difficult to distinguish different labels). However, even for $L = 100$, the performance of our proposal attains a significant improvement compared to the direct approach, where our proposal attains a BER of 0.14, which is a 30 % improvement compared to the BER of 0.2 achieved by the direct approach. Interestingly, for RIS sizes larger than or equal to $N = 16$, the FCN-based approach always reaches nearly optimal throughput and BER irrespective of the number of data labels. These results confirm the robust performance of our proposal for non-small RIS sizes, showing a gap to the optimum lower than 1 %, whereas the direct approach introduces a degradation in throughput higher than 60 % and the random

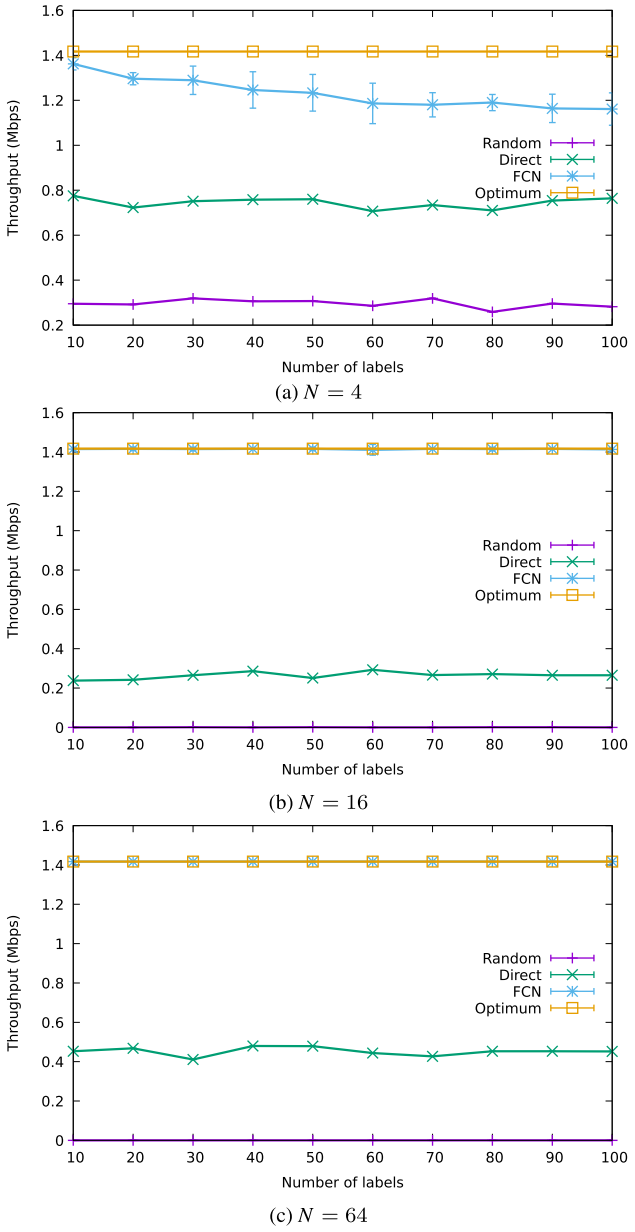

(a) $N = 4$

(b) $N = 16$

(c) $N = 64$

FIGURE 11. Throughput of the FCN, random, direct and optimum approaches for different number of channel labels, for three different RIS sizes ($N = 4, 16, 64$).

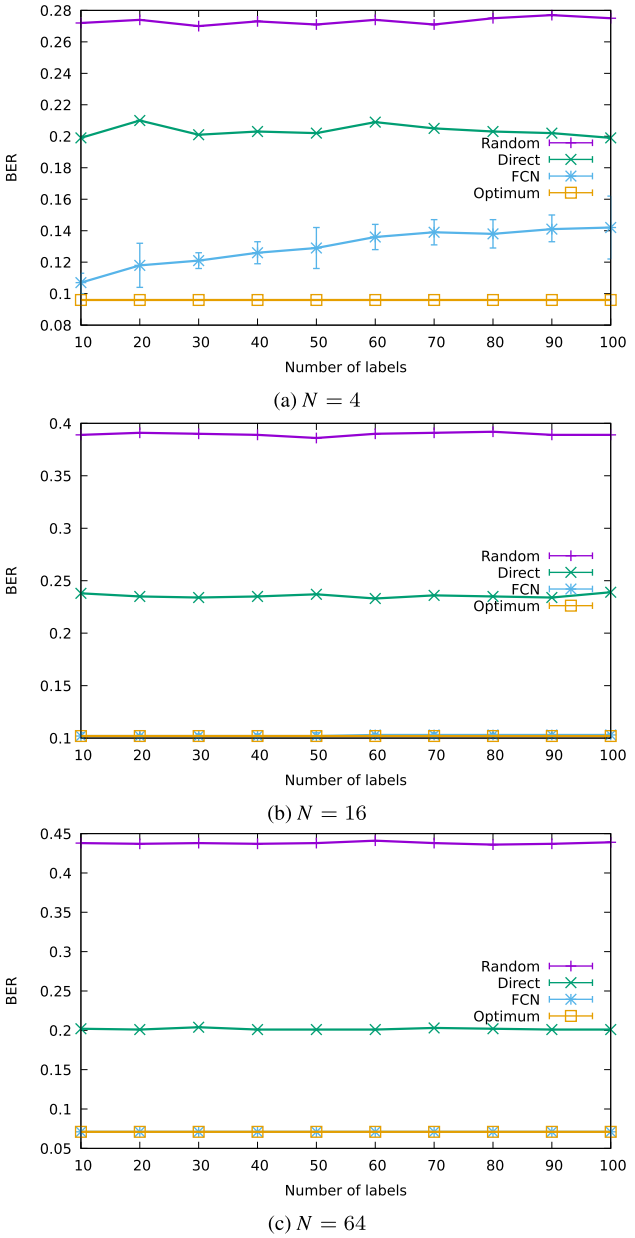

(a) $N = 4$

(b) $N = 16$

(c) $N = 64$

FIGURE 12. BER for the FCN, random, direct and optimum approaches using different numbers of labels.

approach cannot provide a throughput higher than 0. Note that further increasing the number of data labels beyond 100 will require using a higher number of samples for maintaining the performance.

Overall, these results show that our proposed FCN-based approach can be used to reach a close to optimum performance, significantly outperforming baseline approaches such as random phase shifts or direct usage of imperfect CSI. Our results for RIS sizes of 4, 16 and 64 elements show that the throughput and BER achieved by the FCN approach improve when the RIS size increases, at the cost of a longer training time.

VI. CONCLUSION

RIS technology is envisioned to play a pivotal role in future mobile networks. It can be used to adaptively manipulate the phase shift of each reflecting element according to the wireless channel conditions to focus the signal at an intended location. However, determining the optimal phase shift configuration for a given scenario is challenging since an accurate CSI is needed and the number of RIS elements is typically high. On the other hand, the optimization of RIS using imperfect CSI has a non-negligible impact in the achievable performance of the system.

In this paper, we proposed a novel FCN-based approach for estimating the optimal RIS phase shift configuration

from imperfect CSI measurements. Our experimental results demonstrated that our proposed FCN model can close the gap to the optimum system performance (e.g., BER and throughput), while baseline approaches (e.g., a random phase shift configuration or applying directly the noisy CSI measurements) prove to be insufficient to sustain the system performance. The proposed solution is robust even for large CEEs and maintains a nearly optimal performance in terms of throughput and BER for RIS sizes larger than 16 elements, with a gap lower than a 1 % to the optimum bound. This is a substantial improvement compared to baseline approaches, which have a gap to the optimum performance higher than 60 %. The performance improvement is however limited in the case of smaller RIS sizes (e.g., $N = 4$), where we can observe a performance degradation up to 15 % compared to the optimum. The computational complexity of the FCN model grows linearly with the RIS size.

REFERENCES

[1] Y. Liu, X. Liu, X. Mu, T. Hou, J. Xu, M. Di Renzo, and N. Al-Dhahir, "Reconfigurable intelligent surfaces: Principles and opportunities," *IEEE Commun. Surveys Tuts.*, vol. 23, no. 3, pp. 1546–1577, 3rd Quart., 2021.

[2] Q. Wu and R. Zhang, "Towards smart and reconfigurable environment: Intelligent reflecting surface aided wireless network," *IEEE Commun. Mag.*, vol. 58, no. 1, pp. 106–112, Jan. 2020.

[3] L. Wei, C. Huang, G. C. Alexandropoulos, C. Yuen, Z. Zhang, and M. Debbah, "Channel estimation for RIS-empowered multi-user MISO wireless communications," *IEEE Trans. Commun.*, vol. 69, no. 6, pp. 4144–4157, Jun. 2021.

[4] P. Yang, L. Yang, and S. Wang, "Performance analysis for RIS-aided wireless systems with imperfect CSI," *IEEE Wireless Commun. Lett.*, vol. 11, no. 3, pp. 588–592, Mar. 2022.

[5] Y. Yang, B. Zheng, S. Zhang, and R. Zhang, "Intelligent reflecting surface meets OFDM: Protocol design and rate maximization," *IEEE Trans. Commun.*, vol. 68, no. 7, pp. 4522–4535, Jul. 2020.

[6] D. Mishra and H. Johansson, "Channel estimation and low-complexity beamforming design for passive intelligent surface assisted MISO wireless energy transfer," in *Proc. IEEE Int. Conf. Acoust., Speech Signal Process. (ICASSP)*, May 2019, pp. 4659–4663.

[7] B. Zheng and R. Zhang, "Intelligent reflecting surface-enhanced OFDM: Channel estimation and reflection optimization," *IEEE Wireless Commun. Lett.*, vol. 9, no. 4, pp. 518–522, Apr. 2020.

[8] A. M. Elbir, A. Papazafeiropoulos, P. Kourtessis, and S. Chatzinotas, "Deep channel learning for large intelligent surfaces aided mm-wave massive MIMO systems," *IEEE Wireless Commun. Lett.*, vol. 9, no. 9, pp. 1447–1451, Sep. 2020.

[9] H. Huang, J. Yang, H. Huang, Y. Song, and G. Gui, "Deep learning for super-resolution channel estimation and DOA estimation based massive MIMO system," *IEEE Trans. Veh. Technol.*, vol. 67, no. 9, pp. 8549–8560, Sep. 2018.

[10] P. Dong, H. Zhang, G. Y. Li, I. S. Gaspar, and N. NaderiAlizadeh, "Deep CNN-based channel estimation for mmWave massive MIMO systems," *IEEE J. Sel. Topics Signal Process.*, vol. 13, no. 5, pp. 989–1000, Sep. 2019.

[11] Z.-Q. He and X. Yuan, "Cascaded channel estimation for large intelligent metasurface assisted massive MIMO," *IEEE Wireless Commun. Lett.*, vol. 9, no. 2, pp. 210–214, Feb. 2020.

[12] J. T. Parker, P. Schniter, and V. Cevher, "Bilinear generalized approximate message passing—Part I: Derivation," *IEEE Trans. Signal Process.*, vol. 62, no. 22, pp. 5839–5853, Nov. 2014.

[13] K. Wei, J.-F. Cai, T. F. Chan, and S. Leung, "Guarantees of Riemannian optimization for low rank matrix recovery," *SIAM J. Matrix Anal. Appl.*, vol. 37, no. 3, pp. 1198–1222, Jan. 2016.

[14] H. Zhou, M. Erol-Kantarci, Y. Liu, and H. V. Poor, "A survey on model-based, heuristic, and machine learning optimization approaches in RIS-aided wireless networks," *IEEE Commun. Surveys Tuts.*, vol. 26, no. 2, pp. 781–823, 2nd Quart., 2024.

[15] C. Pan, H. Ren, K. Wang, W. Xu, M. Elkashlan, A. Nallanathan, and L. Hanzo, "Multicell MIMO communications relying on intelligent reflecting surfaces," *IEEE Trans. Wireless Commun.*, vol. 19, no. 8, pp. 5218–5233, Aug. 2020.

[16] Q. Wu and R. Zhang, "Intelligent reflecting surface enhanced wireless network via joint active and passive beamforming," *IEEE Trans. Wireless Commun.*, vol. 18, no. 11, pp. 5394–5409, Nov. 2019.

[17] C. Huang, A. Zappone, G. C. Alexandropoulos, M. Debbah, and C. Yuen, "Reconfigurable intelligent surfaces for energy efficiency in wireless communication," *IEEE Trans. Wireless Commun.*, vol. 18, no. 8, pp. 4157–4170, Aug. 2019.

[18] Q. Wu and R. Zhang, "Beamforming optimization for wireless network aided by intelligent reflecting surface with discrete phase shifts," *IEEE Trans. Commun.*, vol. 68, no. 3, pp. 1838–1851, Mar. 2020.

[19] C. Huang, G. C. Alexandropoulos, A. Zappone, M. Debbah, and C. Yuen, "Energy efficient multi-user MISO communication using low resolution large intelligent surfaces," in *Proc. IEEE Globecom Workshops (GC Wkshps)*, Dec. 2018, pp. 1–6.

[20] S. Atapattu, R. Fan, P. Dharmawansa, G. Wang, J. Evans, and T. A. Tsiftsis, "Reconfigurable intelligent surface assisted two–way communications: Performance analysis and optimization," *IEEE Trans. Commun.*, vol. 68, no. 10, pp. 6552–6567, Oct. 2020.

[21] K. M. Faisal and W. Choi, "Machine learning approaches for reconfigurable intelligent surfaces: A survey," *IEEE Access*, vol. 10, pp. 27343–27367, 2022.

[22] C. Huang, G. C. Alexandropoulos, C. Yuen, and M. Debbah, "Indoor signal focusing with deep learning designed reconfigurable intelligent surfaces," in *Proc. IEEE 20th Int. Workshop Signal Process. Adv. Wireless Commun. (SPAWC)*, Jul. 2019, pp. 1–5.

[23] H. Song, M. Zhang, J. Gao, and C. Zhong, "Unsupervised learning-based joint active and passive beamforming design for reconfigurable intelligent surfaces aided wireless networks," *IEEE Commun. Lett.*, vol. 25, no. 3, pp. 892–896, Mar. 2021.

[24] Q. Zhang, W. Saad, and M. Bennis, "Millimeter wave communications with an intelligent reflector: Performance optimization and distributional reinforcement learning," *IEEE Trans. Wireless Commun.*, vol. 21, no. 3, pp. 1836–1850, Mar. 2022.

[25] G. C. Alexandropoulos, S. Samarakoon, M. Bennis, and M. Debbah, "Phase configuration learning in wireless networks with multiple reconfigurable intelligent surfaces," in *Proc. IEEE Globecom Workshops (GC Wkshps*, Dec. 2020, pp. 1–6.

[26] M. A. Aygül, M. Nazzal, and H. Arslan, "Deep learning-based optimal RIS interaction exploiting previously sampled channel correlations," in *Proc. IEEE Wireless Commun. Netw. Conf. (WCNC)*, Mar. 2021, pp. 1–6.

[27] S. Zhang, S. Zhang, F. Gao, J. Ma, and O. A. Dobre, "Deep learning optimized sparse antenna activation for reconfigurable intelligent surface assisted communication," *IEEE Trans. Commun.*, vol. 69, no. 10, pp. 6691–6705, Oct. 2021.

[28] E. Hyytiä and J. Virtamo, "Random waypoint mobility model in cellular networks," *Wireless Netw.*, vol. 13, no. 2, pp. 177–188, Apr. 2007.

[29] E. Basar and I. Yildirim, "SimRIS channel simulator for reconfigurable intelligent surface-empowered communication systems," in *Proc. IEEE Latin-American Conf. Commun. (LATINCOM)*, Nov. 2020, pp. 1–6.

[30] G. Bebis and M. Georgiopoulos, "Feed-forward neural networks," *IEEE Potentials*, vol. 13, no. 4, pp. 27–31, Oct. 1994.

[31] S. Pratschner, B. Tahir, L. Marijanovic, M. Mussbah, K. Kirev, R. Nissel, S. Schwarz, and M. Rupp, "Versatile mobile communications simulation: The Vienna 5G link level simulator," *EURASIP J. Wireless Commun. Netw.*, vol. 2018, no. 1, p. 226, Sep. 2018.

[32] J. An, C. Xu, L. Gan, and L. Hanzo, "Low-complexity channel estimation and passive beamforming for RIS-assisted MIMO systems relying on discrete phase shifts," *IEEE Trans. Commun.*, vol. 70, no. 2, pp. 1245–1260, Feb. 2022.

[33] P. Fondo-Ferreiro. *Neural Network (NN)-Based Reconfigurable Intelligent Surface (RIS) Optimization*. Accessed: Oct. 8, 2024. [Online]. Available: https://gti-uvigo.github.io/nn-ris-optimization/

[34] E. Zöchmann, S. Caban, C. F. Mecklenbräuker, S. Pratschner, M. Lerch, S. Schwarz, and M. Rupp, "Better than Rcian: Modelling millimetre wave channels as two-wave with diffuse power," *EURASIP J. Wireless Commun. Netw.*, vol. 2019, no. 1, pp. 1–17, Dec. 2019.

[35] M. F. Møller, "A scaled conjugate gradient algorithm for fast supervised learning," *Neural Netw.*, vol. 6, no. 4, pp. 525–533, Jan. 1993. [Online]. Available: https://www.sciencedirect.com/science/article/pii/S0893608005800565
[36] B. Sharma and P. K. Venugopalan, "Comparison of neural network training functions for hematoma classification in brain CT images," *IOSR J. Comput. Eng.*, vol. 16, no. 1, pp. 31–35, 2014.

PABLO FONDO-FERREIRO received the bachelor's and master's degrees in telecommunication engineering from the University of Vigo, Spain, in 2016 and 2018, respectively, and the Ph.D. degree in information and communication technologies from the University of Vigo, in 2022, funded by a "la Caixa" Foundation fellowship. He is currently a Postdoctoral Researcher with the University of Vigo funded by a Xunta de Galicia fellowship. In October 2022, he joined the Instituto de Telecomunicaçoes, Aveiro, Portugal, for a two year postdoctoral research stay. He has participated in 15 competitive research projects and co-authored more than 20 papers in peer-reviewed journals and international conference proceedings. His research interests include SDN, mobile networks, MEC, and artificial intelligence.

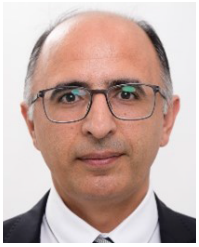

FIROOZ B. SAGHEZCHI (Senior Member, IEEE) received the Ph.D. degree in telecommunications from the University of Aveiro, Portugal, in 2016. He is currently a Senior Researcher with the Chair for Distributed Signal Processing (DSP), RWTH Aachen University, Aachen, Germany. His research contributes to 6GEM research project (6G Research Hub for Open, Efficient and Secure Mobile Communications Systems) funded by the German Federal Ministry of Education and Research (BMBF). Before his current role, he was a Research Fellow (2010–2023) with the Instituto de Telecomunicações, Aveiro, Portugal, and a Lecturer (2003–2010) with Islamic Azad University, Iran. He has authored one book and more than 50 peer-reviewed journals and conference publications and book chapters. His research interests include wireless communications, machine learning, software-defined radio, MIMO signal processing, and radio resource management. He is the Winner of Electronics (MDPI) 2024 Best Paper Award and an Associate Editor of IEEE Access since 2020.

FELIPE GIL-CASTIÑEIRA received the M.Sc. and Ph.D. degrees in telecommunication engineering from the University of Vigo, in 2002 and 2007, respectively. He is currently an Associate Professor with the Department of Telematics Engineering, University of Vigo. Between 2014 and September 2016, he was the Head of the iNetS area in the Galician Research and Development Center in Advanced Telecommunications. He is the Co-Founder of a university spin-off, Ancora. He has published over 60 papers in international journals and conference proceedings. He has led several national and international research and development projects. He holds two patents in mobile communications. His research interests include wireless communication and core network technologies, multimedia communications, embedded systems, ubiquitous computing, and the Internet of Things.

JONATHAN RODRIGUEZ (Senior Member, IEEE) received the Ph.D. degree from the University of Surrey, U.K., in 2004. In 2005, he became a Researcher with the Instituto de Telecomunicações, Portugal, and a Senior Researcher, in 2008. He has served as a Project Coordinator for major international research projects (Eureka LOOP, FP7 C2POWER, and H2020-MSCA-SECRET), whilst acting as the Technical Manager for FP7 COGEU and FP7 SALUS. Since 2017, he has been a Professor in mobile communications with the University of South Wales, U.K. He is currently a Project Director of the NATO SPS-PHYSEC project targeting physical layer security. He is the author of more than 600 scientific works, that include 11 book editorials and currently serving as an Associate Editor for IEEE Access and *IET Communications* journal. His professional affiliations include: a Chartered Engineer (C.Eng.), since 2013, and a fellow of the IET (2015).